PROCEEDINGS OF SCIENCE

Study of the $Z \to ee$ differential cross section as a function of the Z rapidity at $\sqrt{s} = 10$ TeV in CMS

Bryan Dahmes[*†]
University of Minnesota
E-mail: bryan.michael.dahmes@cern.ch

We present estimates for the measurement of the shape of the rapidity distribution for Z bosons produced in proton-proton collisions with the CMS detector at $\sqrt{s} = 10$ TeV and an integrated luminosity of 100 pb^{-1}. The results of this measurement will provide input to constrain the parton density function of the proton at the LHC for many measurements and searches.

XVIII International Workshop on Deep-Inelastic Scattering and Related Subjects
April 19 -23, 2010
Convitto della Calza, Firenze, Italy

[*]Speaker.
[†]On behalf of the CMS Collaboration

PoS(DIS 2010)024

1. Introduction

We present here the expected sensitivity of the measurement of the shape of the rapidity distribution for Z bosons produced at the Large Hadron Collider (LHC) and decaying to e^+e^- pairs recorded by the CMS detector. This measurement provides constraints on the parton density functions (PDFs) at $\sqrt{s} = 10$ TeV which are independent of jet measurement effects and can be directly compared to similar measurements performed at the Tevatron [1, 2].

This measurement is performed by evaluating the following expression for each bin i of the rapidity ($Y \equiv \frac{1}{2}\ln\frac{E+p_z}{E-p_z}$) distribution:

$$\frac{1}{\sigma}\frac{d\sigma(\mathrm{Z}\to \mathrm{e}^+\mathrm{e}^-)}{dY_i} = \frac{(\varepsilon\times A)}{N-B}\cdot\frac{N_i-B_i}{\Delta_i(\varepsilon\times A)_i} = \left[\frac{N_i-B_i}{N-B}\right]\cdot\left[\frac{(\varepsilon\times A)}{\Delta_i(\varepsilon\times A)_i}\right] \tag{1.1}$$

In this expression, $N_i(B_i)$ is the number of Z(background) candidates observed in data, Δ_i is the bin width, and $(\varepsilon\times A)_i$ is the product of the efficiency and acceptance for detecting and fully reconstructing a Z boson with a rapidity within a given Y_i bin.

2. CMS Detector and Monte Carlo Simulation

The CMS experiment is described in detail elsewhere [3]. The central feature of the CMS apparatus is a superconducting solenoid of 6 m internal diameter, providing a uniform magnetic field of 3.8 T. Immersed in the magnetic field are the pixel tracker, the silicon-strip tracker, the leadtungstate crystal electromagnetic calorimeter (ECAL) and the brass/scintillator hadron calorimeter (HCAL). Charged particles are tracked within the pseudorapidity range $|\eta| < 2.5$, where the pseudorapidity is given by $\eta = -\ln\frac{\theta}{2}$ and the polar angle θ of the particle is measured with respect to the anti-clockwise beam direction. In addition to barrel and endcap detectors for ECAL and HCAL which span $|\eta| < 3.0$, the steel/quartz-fiber forward calorimeter (HF), which covers the region $3.0 < |\eta| < 5.0$, was also used for event selection.

The signal $pp \to \mathrm{Z}/\gamma^* + X \to e^+e^- + X$ and Standard Model background Monte Carlo simulation event samples used in this study employed the Pythia 6 [4] event generator. The CTEQ6L1 [5] parton density functions are used to describe parton momenta in the colliding protons. The simulation of the CMS detector response is based on Geant4 [6].

3. Event Selection

$\mathrm{Z}\to\mathrm{e}^+\mathrm{e}^-$ decays are selected from events that first pass the single electron trigger with a transverse energy threshold of 15 GeV. In the selected Z decays, one electron is required to be within the tracking region while the second electron can be found in either the joint acceptance of ECAL and the tracker or in HF. These Z candidates are referred to as ECAL-ECAL and ECAL-HF, respectively. The signal region for both Z types is defined as $70 < m_{ee} < 110\ \mathrm{GeV}/c^2$.

Electrons from Z decays are separated from the rest of the particles in the event using relevant detector information. Fake electrons from hadronic jets generally have neutral and charged components which implies the ECAL shower shape will be wider for jets than for real electrons. Furthermore, the ECAL position for fake electrons often differs from the predicted track position

extrapolated from the collision vertex. We increase the purity of Z electrons by cutting on these quantities and by requiring that the electron candidate be isolated in the tracker and calorimeters.

We reconstruct electrons in HF by taking advantage of the two sets of measurements made in each HF tower [7]. Each tower in the HF is read out by two sets of fibers, one which reads the full depth of the calorimeter ("long" fibers) and one which reads only the deeper portion of the absorber ("short" fibers). Electromagnetic showers lose most of their energy before reaching the short fibers, while hadrons have nearly the same response in both channels. Fake electrons in HF are rejected based on the readout of the long and short fibers. Shower shape information is added to further improve signal purity.

All electron candidates in the final sample must pass the full set of identification and isolation requirements appropriate to the section of the detector involved. The events which include HF, with the associated lack of tracker coverage, have a different background and signal mass resolution. As a result, we consider ECAL-ECAL and ECAL-HF events separately in the analysis, and ECAL-ECAL is given priority if both Z types are found in a single event. A full breakdown of the events by Z type after selection is given in Table 1.

Table 1: Numbers of signal and background events selected by the ECAL-ECAL and ECAL-HF signal definitions after all requirements for 100 pb^{-1}. Background event uncertainties are determined by the number of simulated events available.

Sample	ECAL-ECAL	ECAL-HF
QCD dijets, $20 < p_T < 170$ GeV	24.2 ± 17.1	487.7 ± 76.3
Additional Standard Model processes	79.4 ± 7.6	57.0 ± 8.3
Total Background	103.6 ± 18.7	544.7 ± 76.5
Signal	32500	6283

4. Determination of Single Electron Efficiencies

The efficiencies for the selection criteria and the trigger are determined from data using the "tag-and-probe" method which relies on a sample of $Z \to e^+e^-$ decays that is similar to the analysis sample and contains many of the same events. One "tag" electron must pass strict identification requirements and also be associated with a single electron trigger. The tag electron is combined with a "probe" electron, whose definition depends on the selection requirement under study. The tight tag electron requirements, combined with a dilepton mass constraint, provide a high purity sample of unbiased electrons for measuring individual efficiencies.

For this analysis, it is necessary to bin the efficiencies in variables which may depend on the rapidity of the Z. The most important variables for binning the efficiency are the electron's polar location within the detector (η_d) and its transverse momentum (p_T). Most efficiencies were binned in a single dimension using the variable on which the efficiency has the strongest dependence.

5. Determination of the Efficiency × Acceptance

The individual electron efficiencies, determined as functions of detector space and electron transverse momentum, are combined to yield the total efficiency as a function of Z rapidity. The

$(\varepsilon \times A)$ for each rapidity bin is determined by applying the measured electron efficiencies to Monte Carlo events generated by Pythia and smeared using a fast simulation package tuned to the detector resolutions using Z peak data. This process is effectively a Monte Carlo evaluation of

$$(\varepsilon \times A)_{\mathrm{Z}}(Y) = \int P(\eta_{d+}, \mathrm{p_{T+}}, \eta_{d-}, \mathrm{p_{T-}}; Y)\, \varepsilon_{e^+}(\eta_{d+}, \mathrm{p_{T+}})\, \varepsilon_{e^-}(\eta_{d-}, \mathrm{p_{T-}})\, d\eta_{d+} d\mathrm{p_{T+}} d\eta_{d-} d\mathrm{p_{T-}} \tag{5.1}$$

where $P(\eta_{d+}, \mathrm{p_{T+}}, \eta_{d-}, \mathrm{p_{T-}}; Y)$ is the probability density function for electrons with the given η_{d} and $\mathrm{p_T}$ values for a Z with the given Y and includes the effect of acceptance. The $\varepsilon_{e^\pm}(\eta_{\mathrm{d}}, \mathrm{p_T})$ function represents the total efficiency for an electron with the given detector position and momentum. The final $(\varepsilon \times A)$ distribution is shown in Figure 1. It is clear that the inclusion of HF electrons in this analysis significantly improves the acceptance for this measurement.

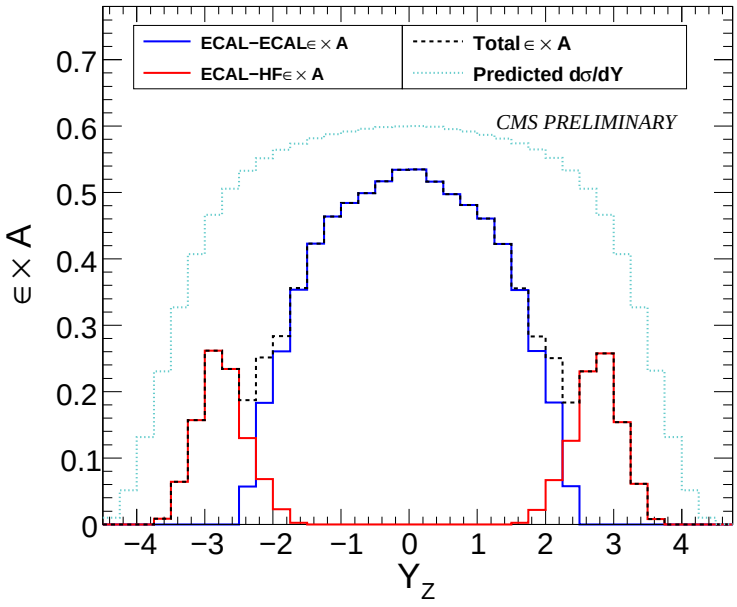

Figure 1: The $(\varepsilon \times A)$ for the signal as determined by convolving the single electron efficiencies using the Monte Carlo distributions for Z electrons.

Besides the $(\varepsilon \times A)$ distribution, the convolution process generates distributions of kinematic variables of the individual leptons as well as the dilepton mass distribution and the transverse momentum of the dilepton system. These distributions have the effects of electron efficiency and acceptance applied to them and thus can be directly compared to both the full Monte Carlo and the data.

6. Evaluation of Systematic Error Contributions

The systematic uncertainties in this measurement arise from the individual efficiencies used in the $(\varepsilon \times A)$ calculation as well as from uncertainties and potential miscalibrations in the Monte Carlo used for the calculation. The effect of each of these uncertainties is propagated to the $(\varepsilon \times A)$

curve. Uncertainties related to the background subtraction are considered as well. The systematic uncertainties are described below and summarized in Figure 2.

The statistical uncertainty from the finite numbers of events available for the efficiency determinations are propagated through the $(\varepsilon \times A)$ calculation. Using the information gathered in the tag-and-probe process, we create pseudoexperiments which use different efficiency distributions created from the base distribution using binomial Bayesian statistics. For each pseudoexperiment, the $(\varepsilon \times A)_i$ is recalculated and normalized by $(\varepsilon \times A)$. The process is repeated several hundred times to determine the effect of statistical uncertainties on the final $(\varepsilon \times A)_i$.

This analysis measurement is sensitive to parton density functions, as deviations from the PDF predictions will result in a change in the distribution of N_i/N from Equation 1.1. However, variation of the parton density functions within PDF parameter uncertainties could act to exaggerate or even cancel the PDF sensitivity. We evaluate the uncertainty due to the variation of $(\varepsilon \times A)_i$ from PDF variation by using the Next-to-Leading Order (NLO) accuracy generator POWHEGz [8] and the CTEQ6.5 PDF set [9]. A fractional difference was calculated for each Y_i bin for each PDF variation relative the median bin value. Contributions of the fractional differences were added in quadrature to produce a cumulative fractional difference.

Final state radiation and several detector effects, such as bremsstrahlung photon emission or the intrinsic resolution of the energy measurement, can alter the reconstructed Z rapidity spectrum as events migrate across the Y_i bin boundaries. The migration effect was studied using Monte Carlo $Z \to e^+e^-$ samples and is limited to a few per cent in most of the rapidity range.

Events with no real $Z \to e^+e^-$ decay which nevertheless pass the selection criteria may alter the appearance of the reconstructed rapidity distribution. We remove QCD and other background processes using a fit to the dielectron mass distribution for events that pass our selection. We describe the background with an exponential function and model the signal $Z \to e^+e^-$ distribution with a Breit-Wigner convolved with a Gaussian. We perform a binned maximum likelihood fit for events with $70 < m_{ee} < 150$ GeV$/c^2$. ECAL-ECAL and ECAL-HF samples are fit separately, and results are combined for Y_i bins which have contributions from both Z types. The results in Figure 2 indicate the importance of background control in the HF region.

7. Results

The final result of the measurement for an integrated luminosity of 100 pb^{-1} is shown in Figure 3 including the raw "data" distribution, the background-subtracted "data" distribution, and the final distribution after the application of the $(\varepsilon \times A)$. Since the underlying physics of the Z rapidity distribution is not expected to have dependence on the sign of the rapidity, we can fold the result around $|Y| = 0$. This process yields the results as shown in Figure 3.

These results include the full shape normalization, including the cancellation of the total cross-section. For comparison, the change in the result expected for a one sigma positive variation of one of the CTEQ PDF vectors (vector 13 [9]) is shown in red in Figure 3. These results indicate the precision of the measurement with 100 pb^{-1} will be sufficient to constrain the PDFs at LHC energies.

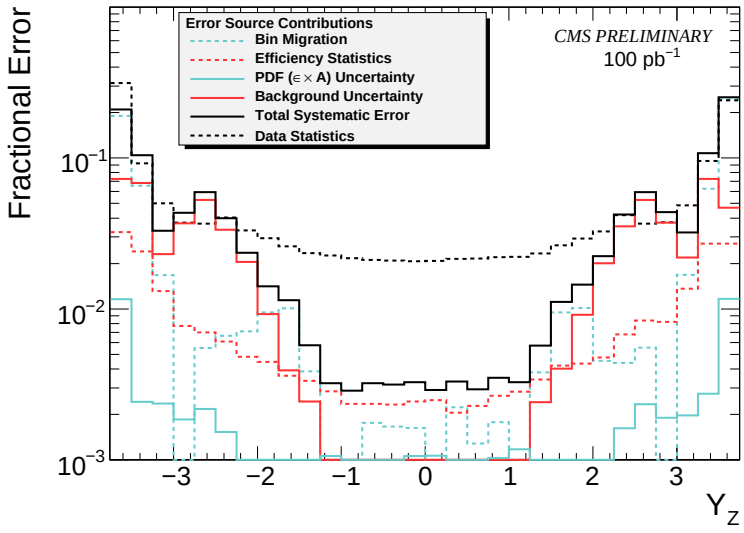

Figure 2: Comparison of the various contributions to the uncertainty in the final measurement as a function of the Z rapidity. The data statistical error for 100 pb^{-1} is shown as a dashed line for comparison.

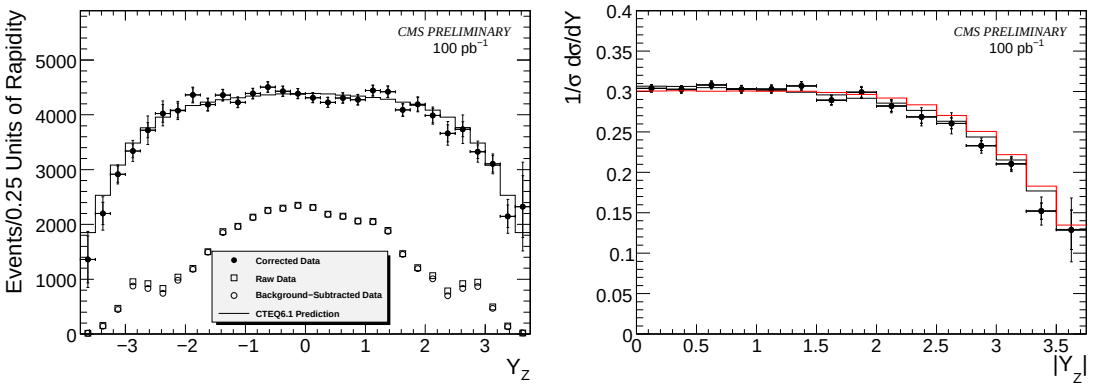

Figure 3: The final results for the rapidity measurement for an integrated luminosity of 100 pb^{-1}. (Left) The raw full simulation ("data") distribution is shown with empty circles and the distribution corrected by $(\varepsilon \times A)$ is shown with solid circles. The errors on the solid circles are shown for statistical and statistical+systematic separately. The prediction of CTEQ6.1 is shown for comparison. (Right) The corrected final result distribution for the rapidity measurement as a function of the absolute value of Z rapidity. The prediction for the positive variation of one of the CTEQ basis vectors (#13[9]) is shown in red.

References

[1] V. M. Abazov *et al.* [D0 Collaboration],
"Measurement of the shape of the boson rapidity distribution for p anti-p → Z / gamma → e+ e- + X events produced at $\sqrt{s}$ of 1.96-TeV,"*
Phys. Rev. D **76**, 012003 (2007).

[2] A. A. Affolder *et al.* [CDF Collaboration],

"Measurement of $d(\sigma)/dy$ for high mass Drell-Yan e^+e^- pairs from $p\bar{p}$ collisions at $\sqrt{s} = 1.8$ TeV,"
Phys. Rev. D **63**, 011101 (2001).

[3] CMS Collaboration,
"The CMS experiment at the CERN LHC,"
JINST 3 (2008) S08004.

[4] T. Sjostrand, S. Mrenna and P. Skands.
JHEP05 (2006) 026 (LU TP 06-13, FERMILAB-PUB-06-052-CD-T).

[5] S. Kretzer, H. L. Lai, F. I. Olness, and W. K. Tung,
"CTEQ6 parton distributions with heavy quark mass effects,"
Phys. Rev. D **69**, 114005 (2004).

[6] Geant4 Collaboration,
"Geant4: a simulation toolkit,"
Nucl. Instrum. and Methods A506 (2003) 250.

[7] G. Baiatian, A. Sirunyan *et al*.
Design, Performance and Calibration of CMS Forward Calorimeter Wedges,
Eur. Phys. J C53: 139-166 (2008).

[8] S.Frixione *et al. Matching NLO QCD computations with Parton Shower simulations: the POWHEG method*, JHEP 0711 (2007) 070, hep-ph/0709.2092.

[9] W.K. Tung *et al. Heavy Quark Mass Effects in Deep Inelastic Scattering and Global QCD Analysis* (2007), hep-ph/0611254.